THE ASTROPHYSICAL JOURNAL, 566:818–832, 2002 February 20

ONGOING MASSIVE STAR FORMATION IN THE BULGE OF M51[1]

H. J. G. L. M. LAMERS,[2,3] N. PANAGIA,[4,5] S. SCUDERI,[6] M. ROMANIELLO,[7] M. SPAANS,[8]
W. J. DE WIT,[2,3] AND R. KIRSHNER[9]
Received 2001 May 3; accepted 2001 May 21

ABSTRACT

We present a study of *Hubble Space Telescope* Wide Field Planetary Camera 2 observations of the inner kiloparsec of the interacting galaxy M51 in six bands from 2550 to 8140 Å. The images show an oval-shaped area (which we call the "bulge") of about $11'' \times 16''$, or 450×650 pc, around the nucleus that is dominated by a smooth "yellow/reddish" background population with overimposed dust lanes. These dust lanes are the inner extensions of the spiral arms. The extinction properties, derived in four fields in and outside dust lanes, are similar to the Galactic extinction law. The reddish stellar population has an intrinsic color of $(B-V)_0 \simeq 1.0$, suggesting an age in excess of 5 Gyr. We found 30 bright pointlike sources in the bulge of M51, i.e., within 110–350 pc from the nucleus. The point sources have $21.4 < V < 24.3$, many of which are blue with $B-V < 0$ and are bright in the UV with $19.8 < m_{2550} < 22.0$. These objects appear to be located in elongated "strings" that follow the general pattern of the dust lanes around the nucleus. The spectral energy distributions of the pointlike sources are compared with those predicted for models of clusters or single stars. There are three reasons to conclude that most of these point sources are isolated massive stars (or very small groups of a few isolated massive stars) rather than clusters:

1. The energy distributions of most objects are best fitted with models of single stars of M_V between -6.1 and -9.1, temperatures between 4000 and 50,000 K, and with $4.2 < \log(L/L_\odot) < 7.2$ and $12\ M_\odot < M_* < 200\ M_\odot$.
2. In the Hertzsprung-Russel diagram the sources follow the Humphreys-Davidson luminosity upper limit for massive stars.
3. The distribution of the sources in the Hertzsprung-Russel diagram shows a gap in the range of $20{,}000\text{K} < T_{\rm eff} < 10{,}000$ K, which agrees with the rapid crossing of the Hertzsprung-Russel diagram by stars, but not of clusters.

We have derived upper limits to the total mass of lower mass stars ($M_* < 10\ M_\odot$) that could be "hiding" within the point sources. For the "bluest" sources, the upper limit is only a few hundred $M_\odot$. We conclude that the formation of massive stars outside clusters (or in very low mass clusters) is occurring in the bulge of M51. The estimated star formation rate in the bulge of M51 is $(1\text{–}2) \times 10^{-3}\ M_\odot\ \text{yr}^{-1}$, depending on the adopted initial mass function. With the observed total amount of gas in the bulge, $\sim 4 \times 10^5\ M_\odot$, and the observed normal gas-to-dust ratio of ~ 150, this star formation rate could be sustained for about $(2\text{–}4) \times 10^8$ yr. This suggests that the ongoing massive star formation in the bulge of M51 is fed/triggered by the interaction with its companion about 4×10^8 yr ago. The star formation in the bulge of M51 is compared with that in bulges of other spirals. Theoretical predictions of star formation suggest that isolated massive stars might be formed in clouds in which H_2, [O I] 63 μm and [C II] 158 μm are the dominant coolants. This is expected to occur in regions of rather low optical depth, $A_V \leq 1$, with a hot source that can dissociate the CO molecules. These conditions are met in the bulge of M51, where the extinction is low and where CO can be destroyed by the radiation from the bright nuclear starburst cluster in the center. The mode of formation of massive stars in the bulge of M51 may resemble the star formation in the early universe, when the CO and dust contents were low because of the low metallicity.

Subject headings: galaxies: bulges — galaxies: individual (M51, NGC 5194) — galaxies: spiral — galaxies: stellar content — stars: evolution — stars: formation

[1] Based on observations with the NASA/ESA *Hubble Space Telescope*, obtained at the Space Telescope Science Institute, which is operated by AURA, Inc., under NASA contract NAS 5-26555.

[2] Astronomical Institute, Princetonplein 5, NL-3584 CC Utrecht, Netherlands; lamers@astro.uu.nl, w.j.m.dewit@astro.uu.nl.
[3] SRON Laboratory for Space Research, Sorbonnelaan 2, NL-3584 CA Utrecht, Netherlands.
[4] Space Telescope Science Institute, 3700 San Martin Drive, Baltimore, MD 21218; panagia@stsci.edu.
[5] On assignment from the Space Science Department of ESA.
[6] Osservatorio Astrofisico di Catania, I-95125, Italy; sscuderi@alpha4.ct.astro.it.
[7] European Southern Observatory, Karl-Schwarzschild Strasse 2, Garching-bei-München, D-85748, Germany; mromanie@eso.org.
[8] Kapteyn Astronomical Institute, University of Groningen, PO Box 800, NL-9700 AV Groningen, Netherlands; spaans@astro.rug.nl.
[9] Harvard-Smithsonian Center for Astrophysics, 60 Garden Street, MS-19, Cambridge, MA 02138; rkirshner@cfa.harvard.edu.

1. INTRODUCTION

The spiral galaxy M51 (NGC 5194, the Whirlpool nebula) and its peculiar companion galaxy NGC 5195 form a typical example of galaxy interaction. After the pioneering hydrodynamical simulations by Toomre & Toomre (1972), several authors have tried to explain the grand design spiral shape and the tidal arms of this interacting system. Hernquist (1990) and Barnes (1998) have critically discussed the successes and the problems of explaining the morphology of the NGC 5194/5195 system, in particular, the radial velocities of the two galaxies, the two-armed spiral structure of M51, the connecting tidal arm, and the large H I arm. The best model is found for a relative orbit that is almost in the plane of M51, for a mass ratio of NGC 5194/5195 $\simeq 2$, a pericenter distance of 17–20 kpc, and a time since pericenter of 2.5×10^8 yr $< t < 4 \times 10^8$ yr (Barnes 1998).

The NGC 5194/5195 system is ideally suited for the study of triggered star formation due to galaxy-galaxy interactions. For this reason, we have started a series of studies on the different aspects of star formation in M51, based on *Hubble Space Telescope* (*HST*) Wide Field Planetary Camera 2 (WFPC2) observations in six broadband filters. The nucleus was studied by Scuderi et al. (2002, hereafter Paper I), who found that it contains a total stellar mass of about $2 \times 10^7\ M_\odot$ within the central 17 pc and a bright point source of $2 \times 10^6\ M_\odot$ within the inner 2 pc. In this paper we study the properties of the elongated "yellow/reddish" region around the nucleus, hereafter called "the bulge," and of 30 bright pointlike sources that we discovered in it. These point sources indicate ongoing star formation in the bulge region, which is otherwise dominated by old (> 5 Gyr) stars (Paper I).

The full *HST*-WFPC2 image of M51 is published in Paper I. The image shows that the nucleus is surrounded by an elongated bulge of about 460 × 860 pc that is dominated by an old stellar population. The spiral arms containing H II regions start outside the bulge. We adopt a distance of $d = 8.4 \pm 0.6$ kpc, corresponding to a distance modulus of 29.62 ± 0.16, which is based on the brightness distribution of planetary nebulae (Feldmeier, Ciardullo, & Jacoby 1997). At this distance, 1″ corresponds to a linear distance of 40.7 pc, one *HST*-Planetary Camera (PC) pixel of 0.″046 corresponds to 1.87 pc, and an *HST*-Wide Field Camera pixel of 0.″1 corresponds to 4.1 pc.

In § 2 we describe the observations and the data reduction. In § 3 we discuss the interstellar extinction in the bulge. In § 4 we describe the properties of 30 bright pointlike sources in this region. In § 5 their energy distributions are compared with those predicted for clusters with different ages and masses and for single stars of different effective temperatures and radii. We will show that most of them are very luminous young stars (single or multiple) rather than clusters. The star formation rate in the bulge of M51 is derived in § 6. In § 7 we compare the formation of massive stars in the bulge of M51 with clusters near the Galactic center, in the interaction region of the Antennae galaxies, and in the bulges of other spiral galaxies. We also discuss the predicted mode of star formation under the conditions that prevail near the nucleus of M51. The conclusions are given in § 8.

2. OBSERVATIONS AND DATA REDUCTION

M51 was observed with *HST*-WFPC2 on 1994 May 12 and on 1995 January 15 as part of the *HST* Supernova Intensive Study (SINS) program to study SN 1994I (see, e.g., Millard et al. 1999). The galaxy was observed through the broadband filters F255W and F336W in 1994 and through the broadband filters F439W, F555W, F675W, and F814W in 1995. We will refer to these filters as the UV, *U*, *B*, *V*, *R*, and *I* filters. The observations in the UV, *U*, and *B* filters were split into four, three, and two exposures of 500, 400, and 700 s respectively, while a single exposure of 600 s was taken with the remaining filters.

The data were processed through the Post Observation Data Processing System pipeline for bias removal and flat-fielding. The removal of the cosmic rays in the UV, *U*, and *B* images was accomplished by combining the available exposures. For the images taken in the other three filters, we used a simple procedure, which consists of combining images obtained in adjacent bands, that allowed us to remove most of the contribution from the cosmic rays (see Paper 1). Unfortunately, the corrected images still showed some residual contamination from cosmic rays, which could have affected the photometry. To obtain a list of the pointlike sources in each filter, we used an unsharp masking method. This was done because of the complexity of the background emission. In fact, it seems that most of the pointlike sources lie on or close to dust lanes that are the inner extensions of the spiral arm structures. The method consisted in smoothing each image using a Gaussian with 4 pixels FWHM and then subtracting the smoothed image from the original image. From each image, the list of sources was obtained by picking up all the objects above a threshold, variable from about 3 to 13 times the local value of the background depending on the filter. These lists contained also residual cosmic rays, so we "cross-correlated" them, selecting only those objects that were present in at least two different filters.

This procedure was applied only to the optical filters. The UV and *U* images were taken 8 months earlier than the optical images, which means that the orientation of the spacecraft was not the same in the two epochs. In the 1995 observations the nucleus of M51 was near the center of the PC images, but in 1994 the images were centered on SN 1994I, and the nucleus was at the edge of the PC image. This means that the UV and *U* observations of about half of the point sources were made with the PC camera, and the rest were made with the Wide Field Camera.

To obtain the photometry of the pointlike sources in the UV and *U* filters, we first took the list containing the positions (pixel coordinates) of the pointlike sources in the optical images and rotated the image, taking the position of SN 1994I as origin, to match the different orientation. In this way we identified the same pointlike sources in the UV images as in the optical images.

We performed aperture photometry using an aperture radius of 2 pixels and calculating the sky background in an annulus with an internal and external radius of 5 and 8 pixels, respectively. The correction for the aperture was obtained from a theoretical point-spread function obtained with TinyTim (Krist & Burrows 1994). The flux calibration was obtained using the internal calibration of the WFPC2, using the spectrum of Vega as the photometric zero point (Whitmore 1995). The uncertainty in the photometry was computed by taking into account photon noise, background noise, and CCD readout noise only. Charge transfer and distortion effects were not taken into account. Tests

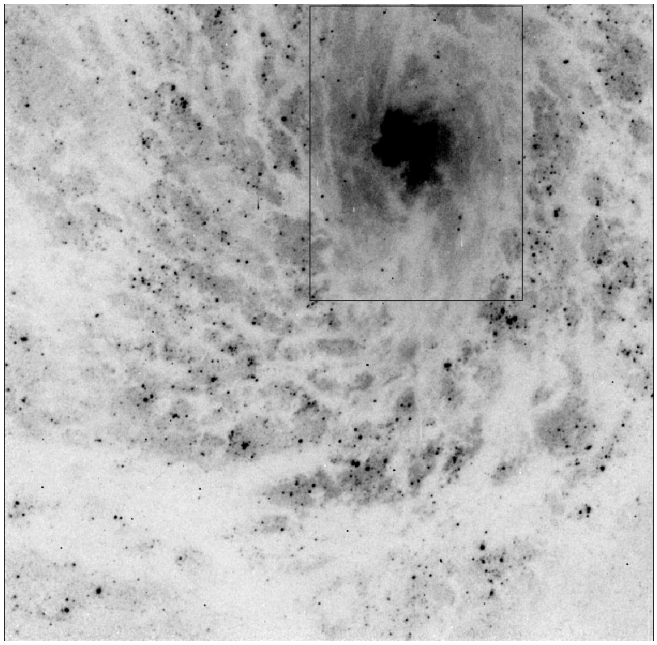

FIG. 1.—Negative F439W image of M51 taken with the *HST*-PC. The field is 36″.8 × 36″.7 or 1.48 × 1.48 kpc. The nucleus and the spiral arms are clearly visible. The rectangle indicates the "bulge region" that is enlarged in Fig. 2. The dust lanes in the bulge follow a spiral structure as if they are the inner extensions of the spiral arms seen at larger distance.

showed that these effects have little influence on the colors (less than about 0.03 mag) and the magnitudes (less than 0.04 mag).

Figure 1 shows the *B* image taken with the Planetary Camera. The bulge region is indicated. Figure 2 shows the region of the bulge enlarged. The symbols and the marked areas are described below.

3. THE INTERSTELLAR EXTINCTION

The region around the nucleus of M51, in an area of about 11″ × 16″ = 460 × 680 pc, appears "yellow/reddish" in the *HST* images. The light from this region, the bulge, is dominated by an old stellar population. The brightness distribution in the bulge is smooth and homogeneous in color apart from the many darker "lanes," which are obviously due to dust extinction (see Fig. 2). Assuming a homogeneous stellar distribution in color and magnitudes, the extinction can be studied by comparing the magnitudes and colors of the dusty regions with those in adjacent regions where the extinction appears to be small.

To this purpose, we have selected in the bulge four areas with different extinctions (fields A–D). The locations of these fields are indicated in Figure 2. For each of the fields, we constructed m_λ versus V and color-color plots of all the pixels. Figure 3 shows the m_λ versus V plots for fields A and C. Assuming that the background population of bulge stars has a uniform color (see Paper I), the slopes of the relations give the extinction ratios. The range of the magnitudes in each field provides an estimate of the maximum extinction values. We find that the extinction in the bulge is small and has a maximum value of about 0.25 in $E(B-V)$, in agreement with Paper I.

The resulting values of the extinction ratios are listed in Table 1, where the values are also compared with the Galactic values for the same *HST* filters based on the extinction curve of Savage & Mathis (1979). The Galactic values were derived by applying the extinction curve to the stellar energy distribution of an unreddened A0 star and then convolving the resulting spectrum with the *HST* filter characteristics (for details, see Romaniello 1998). The table shows that the extinction ratios are quite similar to those of our Galaxy, which suggests that the extinction curves of the two galaxies are about the same. Paper I has reached the same conclusion for the M51 nuclear region but using a somewhat different method.

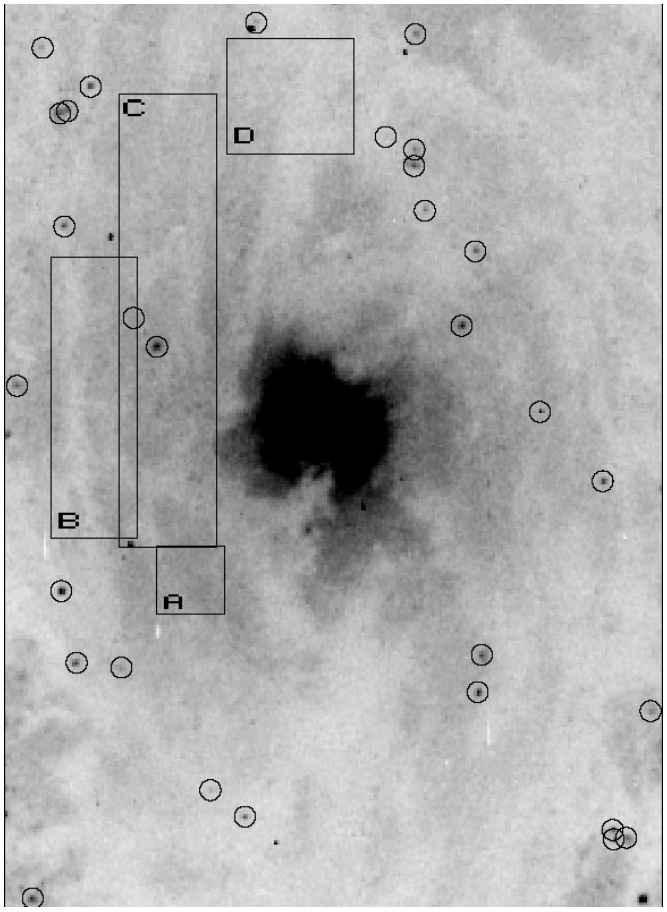

FIG. 2.—Negative F439W image of the region of 11″ × 16″ or 450 × 650 pc around the nucleus of M51 observed with the *HST*-PC camera. Apart from the nucleus and the dust lanes, the region has a smooth structure with colors indicating an old, greater than 5×10^9 yr, population. The four fields, used for studying the extinction curve and the location of the "bulge point sources," are indicated.

TABLE 1

REDDENING IN THE GALAXY AND IN THE BULGE OF M51

Ratio	Galaxy	M51
$E(B-I)/E(B-V)$	2.22	2.14 ± 0.25
$E(V-I)/E(B-V)$	1.52	1.15 ± 0.25
$E(R-I)/E(B-V)$	0.66	0.37 ± 0.15
$A_{UV}/E(B-V)$	6.71	
$A_U/E(B-V)$	5.04	
$A_B/E(B-V)$	4.17	
$A_V/E(B-V)$	3.26	
$A_R/E(B-V)$	2.46	
$A_I/E(B-V)$	1.90	

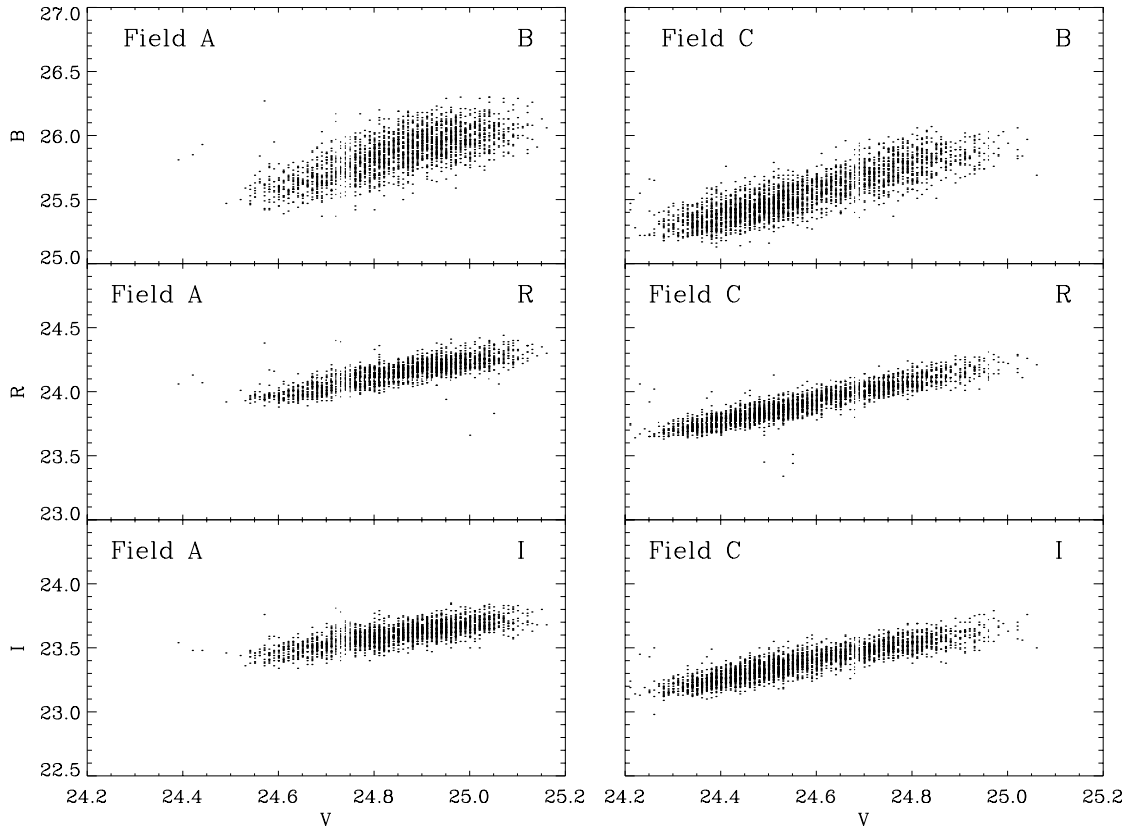

FIG. 3.—The m_λ vs. V plots (in the Vega magnitude system) for the B, R, and I bands of the fields A (*left*) and C (*right*) of the bulge used for the study of the extinction law in the bulge. The slope of these relations define the extinction ratios A_λ/A_V.

Hill et al. (1997) have shown on the basis of a study of H II regions observed with the *Ultraviolet Imaging Telescope* that the far-UV extinction of M51 is smaller than in the Galaxy, $A_{152}/E(B-V) = 6.80$ for M51 compared to 8.33 for the Galaxy. This is not in contradiction with our results because the far-UV extinction at $\lambda < 2100$ Å is known to vary drastically in both the Galaxy and in LMC between different regions.

In the analysis described above we have treated the extinction as a foreground effect. This is justified by the small values of $E(B-V) < 0.25$, for which the effect of the extinction on the flux is independent of the depth distribution of the dust. The fact that we find an extinction curve closely resembling the Galactic one provides additional support to the justification of the adopted method.

4. BRIGHT POINT SOURCES IN THE BULGE

The *HST*-PC image of the central region of M51 (see Fig. 2) shows the presence of bright pixel-size spots, with $21.4 < V < 24.4$. We have estimated the sizes of the sources using radial profile fitting of the F555W images. The vast majority, 21 of 30, are definitely point sources. Six sources have too high a background to allow a reliable size determination. All of them are rather blue, with $B-V < 0.32$ (see below). Two sources (11 and 13) are possibly extended, but they have a low peak count rate and are rather faint. One of these, source 11, is a very red source, with $B-V = 1.8$, whereas source 13 is a blue source, with $B-V = -0.09$ (see below). Only one source, source 4 with $B-V = 0.90$, is definitely resolved. If its intrinsic intensity distribution is Gaussian, it has an intrinsic FWHM of 0.″06, which corresponds to 2.4 pc at the distance of M51. Assuming that the sample of sources that have no reliable FWHM determination contains the same fraction of extended sources as the rest, we conclude that our sample may contain no more than four extended sources. Hereafter, the sources will be called "bulge point sources."

Could the bulge point sources be background galaxies? Using the number and magnitude distribution of galaxies in the Hubble Deep Field (Williams et al. 1996), Gonzalez et al. (1998) derived the expected number and brightness distribution of background galaxies in the *HST*-WF chips of an observation similar to the ones of M51. Our detection limit is about 23.5 mag in V and I due to the bright background of the old stellar background population in the bulge. From the study of Gonzalez et al. (1998) we find that about 13 background galaxies in V and 25 in I above the detection limit are expected in the three WF chips together. The bulge of M51 covers an area that is only 17% of the PC chip and 1.5% of the three WF chips together. So we expect that the bulge image contains about 0.2 background galaxies in V and 0.3 in I. Moreover, background galaxies would not be point sources. Even the extended source 4, with its FWHM of 0.″6, is too small to be a background galaxy (unless it is a quasi-stellar object). It is most likely a small cluster.

4.1. *The Location of the Bulge Point Sources*

The location of the bulge point sources is indicated in Figure 2. The points are not randomly distributed but seem to be located preferentially in an ellipse (with major axis running from the upper left to lower right) or in strings

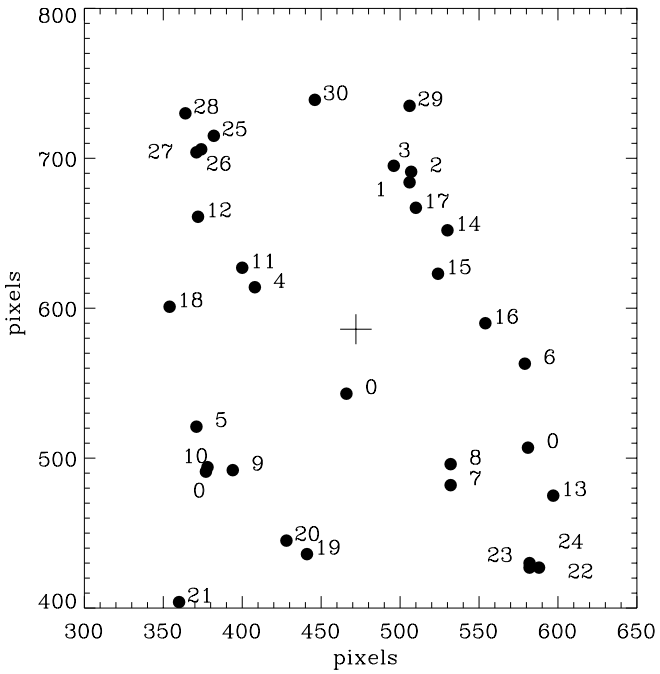

FIG. 4.—Location and the numbers of the 30 point sources in the bulge of M51 that are studied in this paper. Sources with number zero were in the original selection (see Fig. 2) but were not studied because of the lack of reliable photometry. The cross indicates the location of the nucleus of M51 (Paper I). The orientation is the same as in Fig. 2

around the nucleus. This agrees with the general appearance of the region around the nucleus as observed in the B filter: the darker lanes also indicate spiral arms that can be traced down to the nucleus. The main spiral arms originate at a larger distance $\sim 13''$ (~ 500 pc) from the nucleus, i.e., just outside the range of Figure 2 (see Fig. 1).

Figure 4 shows the locations and the numberings of the point sources. From the originally selected 33 sources, three have been removed because we could not derive reliable photometry. These are indicated by the number zero. The numbers of the remaining 30 other sources are indicated. The coordinates of the sources are listed in Table 2.

4.2. *Photometry of the Bulge Point Sources*

The integrated fluxes of the point sources were measured in the UV, U, B, V, R, and I bands, as described in § 2, and converted into Vega magnitudes, where $\mathrm{UV} = U = B = V = R = I = 0$ for Vega (Whitmore 1995). Fourteen of the 30 point sources could not be measured in the UV and U bands because they are too faint. For these point sources, we adopted safe brightness upper limits of $\mathrm{UV} = 21.4$ and $U = 22.3$, which correspond to the magnitudes (minus its uncertainty) of the faintest point sources that were detected in the UV- and U-band images. Sources 26 and 27, which are located close together, could not be measured separately in the UV and U images of the WF chips. We measured the combined magnitudes of the two sources: $\mathrm{UV} = 19.79 \pm 0.11$ and $U = 20.51 \pm 0.06$. These two sources are resolved in the other bands, where they are in the PC chip. Since the energy distributions of the two sources in the B, V, R, and I bands are very similar with a mean magnitude difference of 0.30, we adopt the same difference for the UV and U magnitudes and derived the magnitudes of the two individual sources. The magnitudes of all bulge point sources are listed in Table 2.

Most sources have $B-V$ colors between -0.5 and 1.0 with two red exceptions near $B-V \simeq 2.0$ (sources 3 and 11) and one very uncertain blue exception, namely, source 16 with $B-V = -2.5$. Most sources with $B-V < 0.5$ are detected in the UV and U bands. The three bluest UV sources are sources 12, 26, and 27, which have $-2.1 < U-V < -1.7$ and $-3.1 < \mathrm{UV}-V < -2.6$. These must be hot objects with little or no extinction. The colors of the majority of the point sources, in the range of $-0.3 \leq B-V \leq 1.0$, correspond to spectral types between O and G5, if there were no extinction. The reddest point sources, sources 3 and 11, have $B-V = 2.2$ and 1.8, respectively, which correspond to unreddened M stars.

5. MODELING THE ENERGY DISTRIBUTION OF THE BULGE POINT SOURCES

The bulge point sources have visual magnitudes between 21.4 and 24.4 corresponding to $-8.2 < M_V < -5.2$ if there were no extinction. For a mean reddening of $E(B-V) \simeq 0.3$ (see below), the absolute magnitudes are about $-9.1 \leq M_V \leq -6.1$. This means that the bulge point sources could be either small clusters or very bright stars. We will consider both possibilities.

5.1. *Bulge Point Sources as Clusters*

If the blue point sources are clusters, they cannot be very massive. For instance, a cluster with an initial mass of 10^6 $M_\odot$ and an age of 2×10^6 yr will have a visual absolute magnitude of $M_V = -15.3$ (Leitherer & Heckman 1995). At the distance of M51 and with an extinction of $E(B-V) = 0.3$, the cluster will have $V \simeq 15.3$. The observed point sources are 7–9 mag fainter, so their initial mass must have been a few time 10^2 to a few times 10^3 $M_\odot$. For clusters of such a small mass, the colors and magnitudes cannot be accurately predicted because they will depend on the evolutionary stage of one or a few of the most luminous and most massive stars. Therefore, the results of fitting the observed energy distributions to models should only be considered as a rough estimate of the cluster parameters.

We have fitted the observed energy distributions of the bulge point sources with those predicted for instantaneously formed clusters from Leitherer & Heckman (1995, hereafter "LH models") and from the Frascati group (see below; hereafter called the "Frascati models").

We adopted the LH models of clusters with solar metallicity, with an initial mass function (IMF) of $\alpha = 2.35$ (Salpeter's value) and with an upper mass cutoff of 100 $M_\odot$ and a lower mass cutoff of 1 $M_\odot$. These models cover an age range from 0.2 to 300 Myr. The predicted magnitude in the F255W band was derived from their magnitude at 2100 Å and the slope of the spectral energy distribution between 2100 and 3000 Å. The Frascati models were calculated by M. Romaniello from the evolutionary tracks of Brocato & Castellani (1993) and Cassisi, Castellani, & Straniero (1994) using the WFPC2 magnitudes derived from the stellar atmosphere models by Kurucz (1993). These models are for instantaneous formation of a cluster of solar metallicity stars in the mass range of 0.6–25 $M_\odot$, distributed according to Salpeter's IMF. These models cover an age range of 10–5000 Myr. The LH models are expected to be more accurate for the younger clusters because they are based on the evolutionary tracks of the Geneva group that include

TABLE 2

COORDINATES AND PHOTOMETRY OF BULGE POINT SOURCES

Sourec	R. A. (2000.0)	Decl. (2000.0)	UV F255W (2557 Å)	*U* F336W (3327 Å)	*B* F439W (4292 Å)	*V* F555W (5252 Å)	*R* F675W (6735 Å)	*I* F814W (8269 Å)	$B-V$
1	13 29 52.2747	47 11 45.516	21.27 ± 0.25	21.02 ± 0.07	22.75 ± 0.05	22.40 ± 0.07	22.14 ± 0.10	21.93 ± 0.13	0.33
2	13 29 52.2686	47 11 45.557	...	...	23.52 ± 0.11	23.29 ± 0.15	23.28 ± 0.31	23.16 ± 0.47	0.23
3	13 29 52.2862	47 11 46.108	...	...	25.53 ± 0.54	23.36 ± 0.12	22.26 ± 0.08	21.61 ± 0.07	2.17
4	13 29 52.8049	47 11 45.383	...	...	22.43 ± 0.05	21.53 ± 0.02	20.87 ± 0.02	20.41 ± 0.03	0.90
5	13 29 53.1731	47 11 42.811	23.10 ± 1.69	22.40 ± 0.16	22.17 ± 0.04	21.38 ± 0.02	21.06 ± 0.03	20.95 ± 0.05	0.97
6	13 29 52.3061	47 11 39.177	21.02 ± 0.26	21.61 ± 0.10	23.19 ± 0.09	23.38 ± 0.17	23.35 ± 0.27	23.66 ± 0.47	−0.19
7	13 29 52.6777	47 11 37.339	...	...	22.67 ± 0.07	22.25 ± 0.06	21.88 ± 0.08	21.68 ± 0.11	0.42
8	13 29 52.6364	47 11 37.829	21.00 ± 0.29	21.36 ± 0.08	22.80 ± 0.07	22.79 ± 0.14	22.74 ± 0.18	22.34 ± 0.19	0.01
9	13 29 53.1562	47 11 41.141	...	...	23.80 ± 0.13	23.00 ± 0.09	22.42 ± 0.08	22.14 ± 0.11	0.80
10.....	13 29 53.2188	47 11 41.646	21.18 ± 0.31	21.54 ± 0.09	22.67 ± 0.06	22.56 ± 0.10	22.61 ± 0.19	22.60 ± 0.28	0.11
11.....	13 29 52.8024	47 11 46.045	...	...	25.46 ± 0.51	23.63 ± 0.16	22.81 ± 0.13	21.99 ± 0.11	1.83
12.....	13 29 52.8191	47 11 47.992	20.00 ± 0.19	21.00 ± 0.08	23.13 ± 0.08	23.07 ± 0.14	23.28 ± 0.27	23.69 ± 0.58	0.06
13.....	13 29 52.4526	47 11 35.415	...	...	23.43 ± 0.09	23.54 ± 0.09	23.38 ± 0.09	22.63 ± 0.09	−0.09
14.....	13 29 52.2687	47 11 43.675	21.92 ± 0.50	21.84 ± 0.14	23.31 ± 0.08	23.12 ± 0.11	22.76 ± 0.10	22.79 ± 0.19	0.19
15.....	13 29 52.3624	47 11 42.759	21.36 ± 0.36	21.69 ± 0.11	22.68 ± 0.05	22.36 ± 0.05	22.49 ± 0.09	22.55 ± 0.19	0.32
16.....	13 29 52.3175	47 11 40.786	...	...	23.70 ± 0.10	26.20 ± 1.42	24.51 ± 0.52	...	−2.50:
17.....	13 29 52.3030	47 11 44.586	21.87 ± 0.48	22.46 ± 0.19	23.93 ± 0.11	24.35 ± 0.32	...	...	−0.42
18.....	13 29 53.0396	47 11 46.165	21.27 ± 0.30	21.96 ± 0.12	23.30 ± 0.09	23.03 ± 0.09	22.93 ± 0.12	22.67 ± 0.16	0.27
19.....	13 29 53.1220	47 11 37.787	...	...	22.97 ± 0.06	22.68 ± 0.06	21.92 ± 0.07	22.08 ± 0.11	0.29
20.....	13 29 53.1444	47 11 38.494	...	...	24.48 ± 0.15	23.62 ± 0.12	23.44 ± 0.14	23.62 ± 0.32	0.86
21.....	13 29 53.4973	47 11 38.653	21.35 ± 0.36	21.59 ± 0.10	22.69 ± 0.06	21.70 ± 0.04	21.01 ± 0.03	20.60 ± 0.03	0.99
22.....	13 29 52.6115	47 11 33.894	21.21 ± 0.31	21.53 ± 0.10	22.74 ± 0.06	22.72 ± 0.09	22.44 ± 0.10	23.10 ± 0.33	0.02
23.....	13 29 52.6134	47 11 33.974	...	...	22.99 ± 0.08	22.77 ± 0.10	22.45 ± 0.13	22.28 ± 0.11	0.22
24.....	13 29 52.6164	47 11 33.927	21.12 ± 0.30	21.85 ± 0.11	23.36 ± 0.12	23.45 ± 0.20	23.93 ± 0.36	23.38 ± 0.33	−0.09
25.....	13 29 52.6549	47 11 49.737	...	...	23.14 ± 0.09	23.00 ± 0.09	23.11 ± 0.13	23.05 ± 0.20	0.14
26.....	13 29 52.7204	47 11 49.649	20.40 ± 0.16	21.11 ± 0.11	22.64 ± 0.07	22.79 ± 0.11	23.18 ± 0.20	22.81 ± 0.28	−0.15
27.....	13 29 52.7196	47 11 49.647	20.70 ± 0.21	21.41 ± 0.16	22.91 ± 0.08	23.38 ± 0.16	23.23 ± 0.17	23.19 ± 0.32	−0.47
28.....	13 29 52.6875	47 11 50.763	...	...	23.89 ± 0.11	22.95 ± 0.07	22.34 ± 0.05	21.97 ± 0.07	0.94
29.....	13 29 52.1508	47 11 47.363	21.36 ± 0.38	21.80 ± 0.15	23.60 ± 0.14	23.75 ± 0.19	23.78 ± 0.49	23.11 ± 0.32	−0.15
30.....	13 29 52.3673	47 11 49.068	...	...	23.87 ± 0.12	23.67 ± 0.18	23.56 ± 0.22	23.41 ± 0.26	0.20

NOTE.—Units of right ascension are hours, minutes, and seconds, and units of declination are degrees, arcminutes, and arcseconds. The center of M51 is at pixel (462, 586) and R.A.(2000.0) = $13^h29^m52^s.61$ and decl.(2000) = 47°11′42″.29 (Paper I). The magnitudes are in the Vega system. The average fluxes (in units of ergs cm^{-2} s^{-1} $Å^{-1}$) at the central wavelength corresponding to 0.00 mag are UV = −8.48, U = −8.49, B = −8.17, V = −8.43, R = −8.71, and I = −8.94. Sources not detected in the UV and U bands have brightness upper limits of UV > 21.4 and U > 22.3.

massive stars. The Frascati models are expected to be more accurate for the old clusters because they include stars with masses down to 0.6 $M_\odot$. For both sets of cluster models, the magnitudes were calculated directly from the predicted energy distributions using the WFPC2 filter calibration (Whitmore 1995). These magnitudes will be compared directly with the observed magnitudes, so we do not have to apply the "Holtzman et al." (1995) color correction, which is needed when the magnitudes of the models are given in the standard filters.

For fitting the predicted to the observed energy distributions, we used a three-dimensional maximum-likelihood method. The free parameters are $E(B-V)$, the initial mass M_i, and age t. We corrected the observed magnitudes for extinction in the range of $0.00 < E(B-V) < 2.0$ in steps of 0.02. The extinction values listed in Table 1 were adopted. The weighting factors are chosen as $w_i = 1/(\Delta m_i)^2$, where Δm_i is the uncertainty in the magnitude. For sources that were not detected in the UV and U images, we adopted brightness upper limits of UV > 21.4 and U > 22.3, as discussed above. The uncertainty in the fitting of the UV and U magnitudes to the models depends more strongly on the accuracy of the adopted extinction curve than on the accuracy of the observed magnitudes. This uncertainty of the short wavelength fitting will be larger for objects with large values of $E(B-V)$. To take this into account, we have added an extra term in the uncertainty of $\Delta\mathrm{UV} = 1.5E(B-V)$ and $\Delta U = 1.0E(B-V)$ in the model fitting of the UV and U magnitudes, with a minimum uncertainty of $(\Delta\mathrm{UV})_{\min} = 0.15$ and $(\Delta U)_{\min} = 0.10$. This implies that the fitting had be done in two steps: first, with the normal values of Δm_i to find the best fit of the cluster parameters and $E(B-V)$ and then with the extra uncertainty in the UV and U magnitudes. The values of $E(B-V)$ of the second iteration turn out to be very similar to those of the first iteration.

The resulting fits of the LH models and the Frascati models were compared, and one of the two was adopted based on the following criteria: (1) significantly smaller reduced χ^2_R and (2) a significantly smaller value of $E(B-V)$. This last criterion is used because all reliable fits (small χ^2_R) have a small extinction and because the study of the extinction (see § 3) showed that $E(B-V)$ is very small in the bulge. So if the energy distribution can be fitted with a young cluster of high extinction or an older cluster of low extinction, we adopted the second solution. The uncertainties in the ages and initial masses are derived from the requirement that only fits with $\chi^2_R < \chi^2_R(\min) + 1$ are acceptable. This corresponds to the 68% confidence range.

The results are listed in the left-hand half of Table 3, and the fits are shown in Figure 5*a*. For most sources, a fit with a reasonably small value of $\chi^2_R \lesssim 3$ is found; however, seven sources have a high value of $\chi^2_R > 5$. The cluster parameters

TABLE 3

BULGE POINT SOURCES AS CLUSTERS OR STARS

		CLUSTERS				STARS			
SOURCE	NUMBER BANDS	$E(B-V)$ (mag)	$\log(t)$ yr	$\log(M_i)^a(M_\odot)$	χ^2_R	$E(B-V)$ (mag)	$\log T_{\rm eff}$(K)	$\log L_*(L_\odot)$	χ^2_R
1	6	0.20	$5.35^{+0.80}_{-0.05}$	3.27	3.45	0.64	$4.70^{+0.00}_{-0.22}$	$7.31^{+0.03}_{-0.68}$	0.52
2	4	0.18	$5.35^{+1.30}_{-0.00}$	2.72	0.30	0.36	$4.34^{+0.00}_{-0.44}$	$5.70^{+0.00}_{-0.58}$	0.12
3	4	0.70	$9.70^{+0.00}_{-0.80}$	5.63[b]	0.90	0.50	$3.65^{+0.00}_{-0.00}$	$5.23^{+0.02}_{-0.04}$	0.10
4	4	0.48	$8.70^{+0.08}_{-0.22}$	5.28[b]	0.39	0.70	$3.85^{+0.27}_{-0.00}$	$5.96^{+0.75}_{-0.00}$	0.12
5	6	0.00	$8.90^{+0.00}_{-0.06}$	4.85[b]	14.47	0.02	$3.78^{+0.00}_{-0.00}$	$5.18^{+0.07}_{-0.02}$	9.09
6	6	0.00	$6.20^{+0.00}_{-0.00}$	2.46	2.18	0.10	$4.48^{+0.18}_{-0.10}$	$5.66^{+0.57}_{-0.32}$	0.13
7	4	0.00	$8.74^{+0.00}_{-0.09}$	4.43[b]	0.03	0.24	$3.85^{+0.27}_{-0.00}$	$5.10^{+0.76}_{-0.02}$	0.12
8	6	0.12	$6.60^{+0.00}_{-0.00}$	2.72	0.40	0.38	$4.60^{+0.10}_{-0.26}$	$6.58^{+0.40}_{-0.76}$	0.88
9	4	0.00	$9.18^{+0.00}_{-0.18}$	4.48[b]	0.08	0.24	$3.78^{+0.60}_{-0.04}$	$4.84^{+1.82}_{-0.22}$	0.18
10.....	6	0.18	$6.45^{+0.00}_{-0.10}$	2.79	0.70	0.24	$4.30^{+0.02}_{-0.00}$	$5.75^{+0.07}_{-0.03}$	0.10
11.....	4	0.46	$9.65^{+0.00}_{-1.48}$	5.08[b]	1.40	1.32	$3.90^{+0.80}_{-0.33}$	$5.87^{+2.30}_{-1.07}$	1.10
12.....	6	0.00	$5.60^{+0.25}_{-0.00}$	2.64	12.49	0.00	$4.70^{+0.00}_{-0.00}$	$6.17^{+0.13}_{-0.00}$	3.12
13.....	4	0.02	$7.25^{+0.05}_{-0.00}$	2.82	3.23	0.18	$3.88^{+0.10}_{-0.03}$	$4.59^{+0.33}_{-0.21}$	30.18
14.....	6	0.28	$6.20^{+0.20}_{-0.85}$	2.88	1.58	0.54	$4.70^{+0.05}_{-0.22}$	$6.65^{+0.20}_{-0.66}$	0.51
15.....	6	0.02	$6.65^{+0.00}_{-0.20}$	2.76	5.00	0.34	$4.30^{+0.40}_{-0.15}$	$5.93^{+1.15}_{-0.52}$	3.19
16.....	3	...	...	...	...	...	...	...	...
17.....	4	0.00	$7.00^{+0.00}_{-0.00}$	2.71[b]	6.15	0.00	$4.36^{+0.24}_{-0.00}$	$4.96^{+0.89}_{-0.00}$	0.61
18.....	6	0.22	$5.30^{+0.30}_{-0.30}$	2.89	0.32	0.52	$4.70^{+0.00}_{-0.30}$	$6.90^{+0.05}_{-0.90}$	0.41
19.....	4	0.20	$7.48^{+1.34}_{-0.00}$	3.65[b]	18.73	0.14	$3.81^{+0.00}_{-0.00}$	$4.88^{+0.05}_{-0.05}$	20.54
20.....	4	0.00	$8.85^{+0.00}_{-0.37}$	3.88[b]	5.63	0.00	$3.78^{+0.00}_{-0.00}$	$4.22^{+0.10}_{-0.00}$	4.28
21.....	6	0.18	$9.18^{+0.37}_{-0.36}$	5.22[b]	2.86	1.22	$4.65^{+0.05}_{-0.27}$	$8.17^{+0.16}_{-0.77}$	0.63
22.....	6	0.20	$6.45^{+0.00}_{-0.00}$	2.79	1.89	0.30	$4.38^{+0.27}_{-0.23}$	$5.97^{+0.86}_{-0.70}$	1.76
23.....	4	0.20	$6.50^{+0.00}_{-0.00}$	2.95	0.17	0.20	$3.88^{+0.24}_{-0.03}$	$4.86^{+0.66}_{-0.14}$	0.44
24.....	6	0.02	$6.20^{+0.00}_{-0.05}$	2.43	1.47	0.14	$4.48^{+0.22}_{-0.13}$	$5.66^{+0.73}_{-0.48}$	0.57
25.....	4	0.00	$7.54^{+0.00}_{-0.00}$	3.25[b]	11.83	0.06	$4.00^{+0.00}_{-0.05}$	$4.69^{+0.03}_{-0.14}$	1.21
26.....	6	0.00	$6.35^{+0.05}_{-0.00}$	2.58	2.48	0.00	$4.36^{+0.34}_{-0.00}$	$5.49^{+1.06}_{-0.00}$	0.77
27.....	6	0.00	$6.40^{+0.00}_{-0.00}$	2.42	1.98	0.00	$4.36^{+0.24}_{-0.00}$	$5.36^{+0.76}_{-0.00}$	0.99
28.....	4	0.02	$9.40^{+0.00}_{-0.22}$	4.69[b]	0.09	0.34	$3.78^{+0.00}_{-0.00}$	$4.97^{+0.00}_{-0.00}$	0.03
29.....	6	0.00	$5.50^{+0.00}_{-0.00}$	2.42	2.71	0.26	$4.70^{+0.00}_{-0.30}$	$6.36^{+0.17}_{-0.98}$	1.49
30.....	4	0.22	$6.20^{+0.20}_{-0.55}$	2.55	0.05	0.22	$4.00^{+0.30}_{-0.12}$	$4.65^{+0.85}_{-0.33}$	0.02

[a] M_i is the initial mass of the clusters.
[b] Fracsati cluster model was adopted.

of these models are not reliable. The results in Table 3 confirm our previous estimate that the young clusters have a low mass. More than half of the clusters have an initial mass smaller than about 1000 $M_\odot$. Only old clusters with $t > 500$ Myr have $M_i > 10^4\ M_\odot$. This is due to the detection limit. A cluster with an initial mass is below 5×10^3 $M_\odot$ fades below the detection limit at an age of about 300 Myr (Leitherer & Heckmann 1995).

5.2. *Bulge Point Sources as Individual Stars*

We have also fitted the energy distributions of the bulge point sources to those predicted by model atmospheres of Kurucz (1993). For this purpose, we selected 15 models with temperatures ranging from 3750 to 50,000 K and the lowest gravities in the grid of model atmospheres. We realize that the Kurucz blanketed LTE model atmospheres may not be very accurate for the hottest stars where non-LTE effects and atmospheric extension effects may play a role, so these models are not expected to give accurate values of the stellar parameters based on WFPC2 photometry. However, they serve the present purpose of obtaining an indication of the effective temperature and luminosity of the bulge point sources.

The models were fitted to the observations using a three-dimensional maximum-likelihood method. The free parameters are $E(B-V)$, $T_{\rm eff}$, and radius R_*. To fit the observed energy distributions to those of model atmospheres, we corrected the observed magnitudes for extinction in the range of $0.00 < E(B-V) < 2.0$ in steps of 0.02 (similar to the fit of the cluster models). The resulting dereddened energy distributions were compared to those of the model atmospheres, and the best-fit model was determined. The two fit parameters for the shape of the energy distributions are $E(B-V)$ and $T_{\rm eff}$. The fit parameter for the absolute magnitude is the angular diameter or radius of the star. The weights of the fitting are the same as described in the previous section. To take into account the uncertainty in the extinction at the wavelengths of the UV and U filter, we have added an extra uncertainty ΔUV and ΔU, as described in the previous section.

The results are listed in the right-hand side of Table 3. We list the values of $E(B-V)$, $T_{\rm eff}$, and $\log(L/L_\odot)$ and the value of the reduced χ^2_R of the fit. The range of acceptable parameters was determined in the same way as for clusters; i.e., the acceptable models have $\chi^2_R < \chi^2_R(\min) + 1$. Notice that for almost all sources that are observed in six wavelength bands, the fits of the energy distributions to stellar models are significantly better (smaller χ^2_R) than fits to the cluster models. In total, 23 objects have $\chi^2_R < 3$, and only three have $\chi^2_R > 5$.

The values of $E(B-V)$ derived from the fits are in the range of 0.0–1.3, with more than half of the objects having

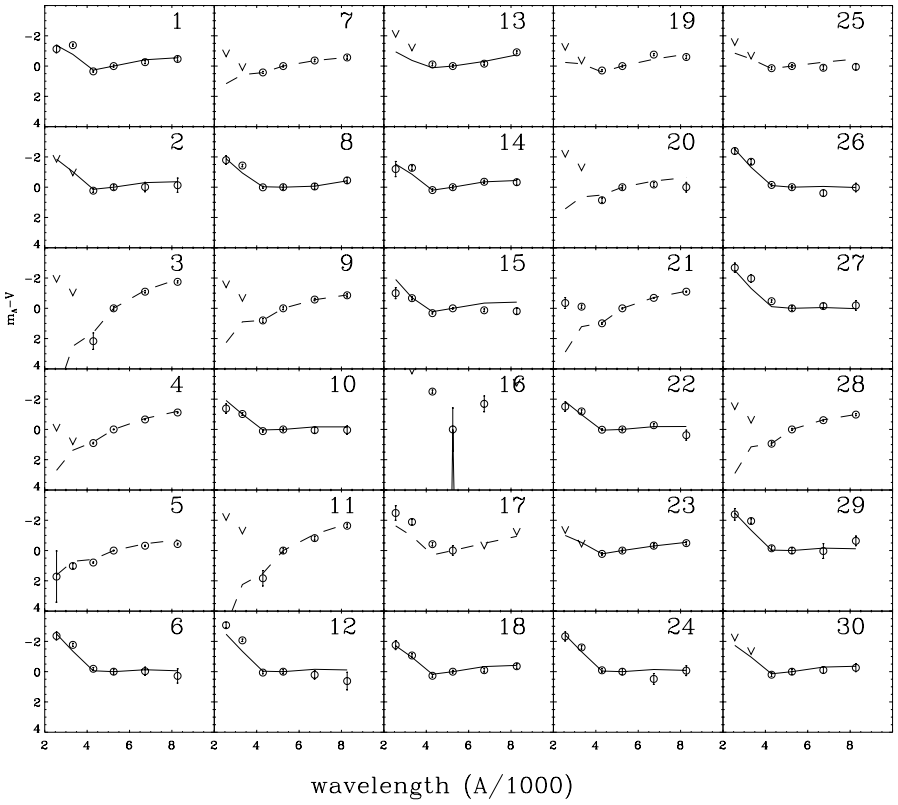

FIG. 5*a*

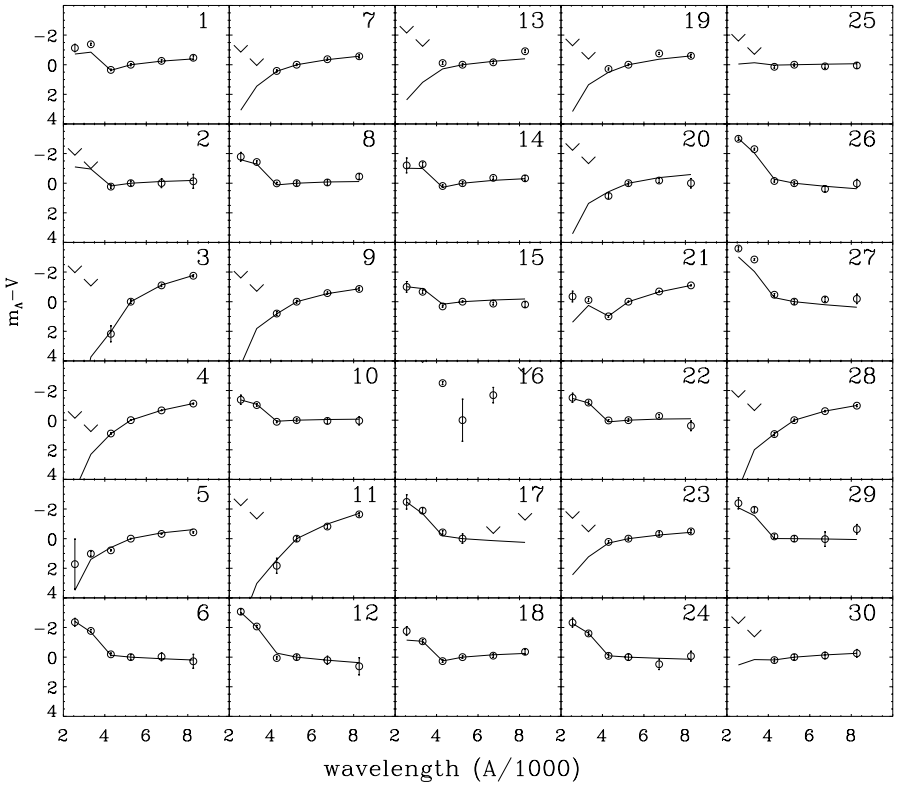

FIG. 5*b*

FIG. 5.—Comparison between the observed magnitudes of the bulge point sources (*circles with error bar*) and the fits of (*a*) cluster models and (*b*) stellar models with extinction. In (*a*) the full lines indicate Leitherer & Heckman (1995) models, and dashed lines indicate Frascati models. Arrows indicate upper limits. The vertical scale is $m_\lambda - V$ in magnitudes, and the horizontal scale is λ(Å)/1000.

$E(B-V) < 0.30$. The uncertainty in the derived values of $E(B-V)$ affects the uncertainty in $T_{\rm eff}$ and log L. A higher value of $E(B-V)$ corresponds to a higher value of $T_{\rm eff}$, a higher value of L_* (because the bolometric correction increases with $T_{\rm eff}$), and a smaller radius of the object. We list the uncertainty in log $T_{\rm eff}$ and log L_* but not in $E(B-V)$. The uncertainty in log L_* is related to the uncertainty in log $T_{\rm eff}$ by $\Delta \log L_* \simeq 6.7\Delta \log T_{\rm eff}$ for the hottest stars with $T_{\rm eff} > 30{,}000$ K and $\Delta \log L_* \simeq 5.3\Delta \log T_{\rm eff}$ for the stars with 10,000 K $< T_{\rm eff} < 30{,}000$ K. For stars in the range of 5000 K $< T_{\rm eff} < 10{,}000$ K, the bolometric correction (BC) is very small and almost independent of $T_{\rm eff}$. For the coolest point source in our sample, i.e., source 3, the BC is sensitive to $T_{\rm eff}$, but the uncertainty in the derived value of $T_{\rm eff}$ is very small. Typical uncertainties are $\Delta E(B-V) \simeq 0.10$, $\Delta \log T_{\rm eff} \simeq 0.1$, and $\Delta \log L_* \simeq 0.4$ for hot stars observed in all six bands and $\Delta E(B-V) \simeq 0.20$, $\Delta \log T_{\rm eff} \simeq 0.2$, and $\Delta \log L_* \simeq 0.6$ for the cooler stars observed in the visual colors only. For stars with $T_{\rm eff} >$ 30,000 K, the uncertainty is larger (possibly as large as 10,000 K at $T_{\rm eff} > 40{,}000$) because of the uncertainties in the adopted Kurucz (1993) model atmospheres.

Figure 5*b* shows the comparison between the observed magnitudes and the predicted magnitudes of the best-fit model for each point source as a function of wavelength. The observed lower limits are also indicated. Notice that the agreement is satisfactory for almost all models. We discuss the following typical energy distributions:

1. Source 3 is the reddest object in our sample. It fits the energy distribution of a cool star of $T_{\rm eff} = 4500$ K with a large extinction of $E(B-V) = 0.50$.

2. Sources 12, 26, and 27 are the three objects with the brightest relative UV magnitude in our sample. They have an energy distribution of a hot star of $T_{\rm eff} = 50{,}000$ K (source 12) or 23,000 K (sources 26 and 27) without extinction.

3. Source 20 is a cold star of $T_{\rm eff} = 6000$ K without extinction. The sharp decrease in flux to shorter wavelength agrees with the observed upper limit of the flux in the UV and *U* band.

4. If source 21 is a hot but heavily extincted star, as suggested by the fit, its luminosity is so high that it must be a cluster. The cluster fitting showed that it could be an old cluster. Surprisingly, however, the FWHM of this source shows that it is a point source. Maybe it is a very cool star.

From studies of Galactic early-type stars, it is known that about half of the luminous stars are in binary systems with a mass ratio close to unity (Garmany, Conti, & Massey 1980), so we can expect that a significant fraction of the bulge point sources are, in fact, binaries. Since the post–main-sequence lifetime is much shorter than the main-sequence lifetime, it is most likely that the systems are observed when either both stars are on the main sequence or one of the two stars has already finished its life. So, with a few exceptions (less than about 10%), we can expect that the energy distribution of a binary system will be close to that of a single star with a luminosity, at most, twice as high as that a single star.

Figure 6 shows the resulting HR diagram of the bulge point sources. One object, source 21 with log $T_{\rm eff} = 4.65$ and log $(L_*/L_\odot) = 8.17$, is outside the range of the figure. An uncertainty in $E(B-V)$, and correspondingly in $T_{\rm eff}$ and

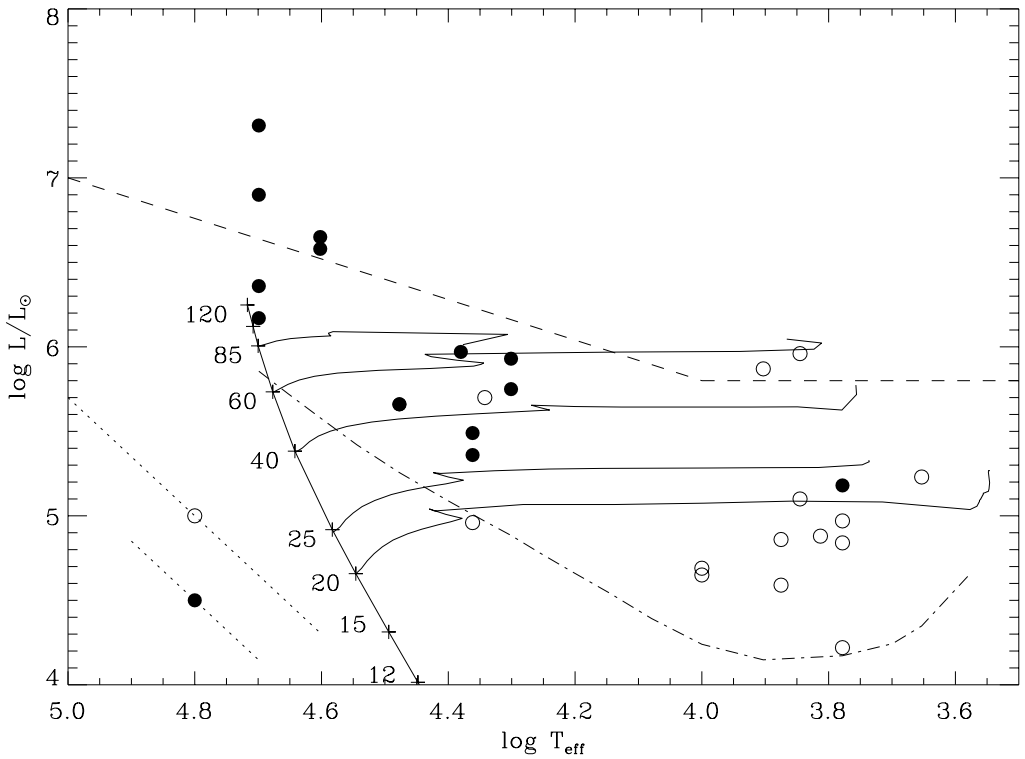

FIG. 6.—HR diagram with the point sources in the bulge of M51, under the assumption that they are single stars. The open circles refer to stars that were not detected in the F255W and the F336W images. Typical error bar are indicated. The solid lines are the evolutionary tracks for Galactic stars with enhanced mass-loss rates from Meynet et al. (1994). The main sequence is indicated with initial masses. The dashed line is the Humphreys-Davidson luminosity upper limit for Galactic stars. The dash-dotted line is the predicted detection lower limit for unreddened stars of $V = 24.0$.

log L_* for a fixed value of V, results in tilted error bars because a higher $E(B-V)$ implies a higher temperature and a larger bolometric correction. We show only the typical error bars since the individual values can be derived from Table 3. The figure also shows part of the evolutionary tracks of massive stars for Galactic metallicities from Meynet et al. (1994) for enhanced mass-loss rates. We see that *if* the point sources are indeed single stars, their initial masses are in the range of about 12–150 $M_\odot$. The four brightest objects might even have masses of about 200 $M_\odot$ if they are single stars. This is about the same mass as the famous "Pistol star" near the Galactic center (Figer et al. 1998).

The empirical luminosity upper limit for stars, i.e., the Humpreys-Davidson (HD) limit (Humphreys & Davidson 1979; Fitzpatrick & Garmany 1990), is shown in Figure 6. Almost all the bright point sources have luminosities very close to or below the HD limit. This suggests that at least a majority of the bulge point sources could be massive stars. The group of hot stars with $\log T_{\rm eff} \geq 4.30$ and $\log (L_*/L_\odot) \geq 5.5$ have initial masses between about 40 and 150 $M_\odot$ and ages on the order of (4–8) $\times 10^6$ yr or less. The group of cool stars with $\log T_{\rm eff} \leq 4.0$ and $\log (L_*/L_\odot) \leq 5.3$ have initial masses between 15 and 25 $M_\odot$ and ages between 7×10^6 and 17×10^6 yr (Meynet et al. 1994). We note that the radius (or luminosity) of the star was a free parameter in the fitting of the models to the observations, so the luminosity was not restrained by the input models.

The two hot objects high above the HD limit in Figure 6 are the following:

1. Source 1, with $4.48 < \log T_{\rm eff} < 4.70$ and $6.63 < \log (L_*/L_\odot) < 7.34$.
2. Source, 14 with $4.38 < \log T_{\rm eff} < 4.65$ and $5.99 < \log (L_*/L_\odot) < 6.85$.

Source 1 is definitely a point source. Source 14 is in a region of high background radiation, so its FWHM could not be determined. These sources might be either superluminous stars or small clusters. Source 21 is also a cluster, based on its brightness. We note that because of the uncertainties in the Kurucz model atmospheres of high temperature, the hottest objects may have a substantial uncertainty in the determination of $T_{\rm eff}$ and L_*.

The lower limit of the luminosity of the point sources in the HR diagram is due to a combination of three effects: (1) the detection limit, (2) the extinction, and (3) the bolometric correction as a function of intrinsic color. We can predict the location of the lower limit in this diagram if we adopt a magnitude limit of $V < V_{\rm lim} \simeq 24.0$, no extinction, and the BC versus $T_{\rm eff}$ relation from the Kurucz (1993) model atmospheres for Galactic metallicity. The resulting lower limit is shown in Figure 6. It agrees very well with the observations. Stars (or clusters) fainter that this detection limit might be present in the bulge of M51 but would not have been detected.

A striking feature of the distribution of the stars in the Hertzsprung-Russel diagram is the gap in temperature between $\log T_{\rm eff} = 4.0$ and 4.3, apart from the error bar of the sources just outside the gap. The mean value of $\log T_{\rm eff}$ is 4.51 ± 0.16 for the hot group of $\log T_{\rm eff} > 4.2$ and 3.84 ± 0.09 for the cold group of $\log T_{\rm eff} < 4.0$, so the two groups do not overlap. Such a gap in the $T_{\rm eff}$ distribution is expected if the point sources are stars because massive stars cross this temperature interval in a short time after their main-sequence phase. The gap is not expected if the sources were clusters.

5.3. *The Contribution of Low-Mass Stars to the Spectral Energy Distribution of Point Sources*

We found above that the energy distributions of the majority of the sources can best be fitted to that of individual massive stars rather than clusters. Moreover, the vast majority of the objects are point sources (see § 4). This shows that the energy distributions of the objects are dominated by one (or very few) massive star(s). In this section we will try to answer the following question: How many low-mass stars could be hiding near the luminous stars before we would notice their presence in the spectral energy distribution? We will describe two tests.

5.3.1. *Test 1: A Cluster with an IMF Mass Distribution*

Let us consider the case that an observed point source is, in fact, a cluster with a certain IMF. Suppose that the cluster contains one massive star (the observed one), with the derived mass M_* and luminosity L_*, plus a tail of lower mass stars on the main sequence, distributed in mass according to an IMF $N(M) = CM^{-\alpha}$ with $\alpha = 2.35$ (Salpeter's value). In these calculations we adopt a conservative lower mass limit of $M_{\rm min} = 1\ M_\odot$. The constant C is determined from the condition that the most massive star is formed at the median of its probability interval, so that

$$\int_{M_*}^{M_{\rm max}} N(M)dM = \frac{C}{-\alpha+1}\,(M_*^{-\alpha+1} - M_{\rm max}^{-\alpha+1}) = 0.5\ , \tag{1}$$

where $M_{\rm max}$ is the mass upper limit for star formation, which we assume to be about 200 $M_\odot$. This will then also determine the mass of the next massive star, as the solution of the same integral but with M_* replaced by $M_{\rm next}$ and 0.5 by 1.5, etc. If we also assume a mass-luminosity relation $L/L_\odot \propto (M/M_\odot)^\beta$ with $\beta = 3$, we can calculate the total luminosity and the total mass of the cluster.

We found that in a cluster with a most massive star of $M_* = 80\ M_\odot$ the stars with masses $M < 80\ M_\odot$ contribute only about 1% to the luminosity when their total mass is 640 $M_\odot$. For a cluster with a most massive star of 120 $M_\odot$, a total mass of 1100 $M_\odot$ in lower mass stars is needed to increase the luminosity by 1%. This contribution from lower mass stars scales linearly with the mass of the cluster. The mean colors of the total radiation from cluster stars of $M_{\rm min} < M < M_*$ are similar to those of an A-type star, i.e., $BC \simeq B-V \simeq V-R \simeq 0$.

The next question is the following: Can we notice the presence of such a cluster in the energy distribution? To answer this question, we have to look at the long wavelength part of the spectrum, where the contribution of the cool stars may dominate that of the brightest hot star. The most stringent test is provided by the bluest point sources. The bluest source without extinction is source 12, which has $T_{\rm eff} = 50{,}000$ K, $\log L_* = 6.17$, $M_* \simeq 120\ M_\odot$, and a bolometric correction of 4.27. The visual magnitude has an uncertainty of 0.14 (1 σ). If there is a cluster, it should increase the brightness in the V band by less than $3\sigma(V) = 0.42$. Suppose the brightest star (i.e., the observed hot star) has a luminosity of L_* and that the contribution of the cluster to the luminosity is xL_*. It is easy to show that

the visual brightness will increase by a factor

$$\frac{F_V(\text{bright star} + \text{cluster})}{F_V(\text{bright star})} = 1 + x10^{-0.4\text{BC(cluster)} + 0.4\text{BC(star)}}, \quad (2)$$

where the two bolometric corrections are those of the brightest star and of the rest of the cluster. The factor x is thus related to the brightness increase in the V band by

$$x = \frac{10^{+0.4\Delta(V)} - 1}{10^{-0.4\text{BC(cluster)} + 0.4\text{BC(star)}}}, \quad (3)$$

with $\Delta(V) = 3\sigma(V)$. Applying the equation to source 12, we find $x = 0.09$. Using the calculations described above, we find an upper limit to the cluster mass of 840 $M_\odot$. Using the same method for sources 29, 6, 27, and 26, with $T_{\rm eff}$ = 50,000, 30,000, 23,000, and 23,000, respectively, we find upper limits to the mass of the clusters of 1200, 500, 420, and 240 $M_\odot$, respectively. These values are of about the same order as derived from the cluster fits in § 5.1. So sources 26 and 27 with $M_* \simeq 35\ M_\odot$ provide the most stringent upper limits to the mass of the clusters, of only a few hundred $M_\odot$. A similar test for the R-band magnitudes gives almost identical results.

5.3.2. *Test 2: A Cluster with Stars of 1 $M_\odot < M_* < 10\ M_\odot$*

In the second test we have assumed that the luminous star is surrounded by a cluster consisting of stars with masses between 10 and 1 $M_\odot$, distributed according to an IMF with a slope of 2.35. We assumed that the stars are on the zero-age main sequence, and we adopted the *HST* band fluxes calculated by Romaniello (1998) for the Kurucz (1993) model atmospheres to calculate the *HST* magnitudes of such a cluster. For a total cluster mass of 1000 $M_\odot$ at a distance of 8.4 Mpc, we find the following magnitudes (in the Vega system): $m_{\rm bol} = 22.12$, UV = 22.24, $U = 22.76$, $B = 23.70$, $V = 23.78$, $R = 23.82$, and $I = 23.86$. We then fitted the observed energy distributions of those 14 point sources that were observed in all six wavelength bands, with a model energy distribution that had the following properties: it consists of a star with either $T_{\rm eff}$ = 40,000 or 25,000 K (depending on the value of $T_{\rm eff}$ that we found by assuming it to be a single star; see Table 3), with a luminosity of L_* plus a cluster with a total mass of $M_{\rm cl}$. The free parameters of the fitting procedure are L_*, $M_{\rm cl}$, and $E(B-V)$. The fitting was done in exactly the same way as described in §§ 5.1 and 5.2.

For nine of the 14 point sources, we find that the cluster masses of the best-fitting energy distribution are less than 400 $M_\odot$. The energy distributions of sources 6, 12, 14, 15, and 29 are best fitted without clusters ($M_{\rm cl} \leq 20\ M_\odot$). For six of the 14 sources (sources 6, 10, 15, 24, 26, and 27), even the *maximum* cluster mass that is compatible with the observed energy distribution is less than 400 $M_\odot$.

So we conclude that for the majority of the bulge point sources, the energy distribution is dominated by only one (or very few) massive star(s) and that for the hottest sources, the upper limit to the mass of a possible accompanying cluster is surprisingly small.

5.3.3. *Comparison with the Orion Nebula Cluster*

We compare the energy distribution of the hottest and bluest sources of M51 with that expected for the very young Orion Nebula cluster (ONC) if it was at a distance of M51.

In optical and UV images, the ONC cluster with an age of about 3×10^5 yr appears like a group of four bright hot stars with a distribution tail of much fainter and cooler pre–main-sequence stars. At the distance of M51 such a group of a few luminous hot stars might resemble the bulge point sources. In reality, however, the Trapezium stars are members of a larger star-forming cluster with a diameter of about 5 pc with about 1600 optical stars and a total mass in excess of $10^3\ M_\odot$ (Hillenbrand 1997). The main sequence is populated down to $M_V \simeq 2$, corresponding to type A5 and a mass of 2 $M_\odot$. The lower mass stars are still in their pre–main-sequence phase. A large fraction of the stars are reddened by an extinction of A_V = 1.5–8.5 mag. This is much higher than the extinction of the M51 bulge point sources. So the total energy distribution of the ONC stars does not resemble that of the UV brightest bulge point sources.

At an age of a few Myr, when most of the dust around the ONC stars will be dispersed and the lower mass stars have reached the main sequence, the Orion Nebula cluster would look like a "normal" cluster with a well-populated main sequence, weighted toward the low-mass end. We compare the energy distribution of the unreddened ONC with that of the hottest bulge point sources.

Hillenbrand (1997) has determined the stellar parameters of 940 stars of the 1600 ONC stars. She has shown that this is a representative sample of the stars in that cluster. The total mass of these 940 stars is 640 $M_\odot$: about 90 $M_\odot$ for the four hot Trapezium stars and 550 $M_\odot$ for the lower mass stars. These lower mass stars are underrepresented by a factor of 2. We have used the parameters of these 940 stars, together with the energy distributions of the stellar atmospheres (Kurucz 1993), to calculate the energy distribution of the cluster if it was located in M51. The V magnitude of this cluster, in the *HST* Vega system used throughout this paper, would be 23.26 if the stars had no reddening at all. The four hottest stars contribute 84%, 70%, and 58% to the flux in the UV, V, and I bands, respectively. A comparison of the resulting unreddened ONC energy distribution with those of the hottest M51 point sources shows that the spectra of the bluest sources 6, 24, 26, 27, and 29 are compatible (within the uncertainty of the observations) with that of the ONC. The visual magnitudes of these point sources are about the same as expected for the unreddened ONC. So these blue point sources look like the ureddened ONC if the low-mass stars are underrepresented by a factor of 2. If we correct the predicted ONC energy distribution for the factor of 2 undersampling of the low-mass stars, we find that the predicted R and I magnitudes are too bright compared to the observed energy distribution of the hottest bulge point sources. Source 12 is "bluer" than the unredenned ONC, even with the undersampling of the low-mass stars.

We conclude from these tests that the M51 bulge point sources *could* be hiding small clusters. However, for the bluest sources, these clusters must have a total mass of less than about 400 $M_\odot$, whereas the star that dominates the energy distribution is already more massive than about 40 or even 120 $M_\odot$ (source 12).

5.4. *Stars or Clusters?*

We have found that the energy distributions of the bulge point sources can be fitted with those predicted for young massive stars or for young clusters of low total mass based

on the following criteria:

If they are single stars, the initial mass of the hot luminous ones with $\log T_{\rm eff} > 4.3$ and $\log (L_*/L_\odot) > 5.5$ must be larger than about 40 $M_\odot$, and their age must be lower than 4 Myr. The group of stars at $\log T_{\rm eff} < 4.0$ and $4.2 < \log (L_*/L_\odot) < 5.2$ had initial masses between 12 and 25 $M_\odot$ and an age of 7–17 Myr.

If the bulge point sources are clusters, half of the clusters have ages larger than 10 Myr. The other half of the clusters is very young (<4 Myr) with small initial masses between 250 and 2000 $M_\odot$. The spectral energy distributions of these young clusters show that even the clusters with the lowest masses must contain at least one massive hot star.

The following four reasons suggest that the point sources are massive stars or very small groups of a few massive stars or poor clusters whose energy distributions are dominated by one or two massive stars:

1. The single-star models fit the energy distributions systematically better than the cluster models. This can be seen by comparing the values of χ^2_R(min) of the stellar fit and the cluster fit in Table 3 and from Figure 5. Basically, the observed fluxes of the point sources better fit the "narrow" energy distributions of single stars than the "wider" distributions predicted for clusters that contain a range of stars of different masses and temperatures.
2. Half of the objects are very hot and should contain at least one or several massive O stars in the range of 40–120 $M_\odot$ to explain the UV magnitudes. The tests described above show that *if* the point sources are clusters, the cluster mass in the form of lower mass stars is less than about 400 $M_\odot$ for the six UV-brightest objects.
3. The point sources follow the Humpreys-Davidson luminosity upper limit in the HR diagram with a few exceptions. This is to be expected in case the point sources are stars, but there is no reason why clusters would follow this stellar upper limit in the HR diagram.
4. The location of the sources in the HR diagram shows a division of the temperature distribution into two separate groups: one with $\log T_{\rm eff} > 4.30$ and one with $\log T_{\rm eff} < 4.0$. This is to be expected if the point sources are stars because the temperature range between the main sequence and the red supergiants in the HR diagram is crossed rapidly by stellar evolution but not if the point sources were clusters.

We realize that the number of sources is small and that we cannot fully exclude the possibility that arguments 3 and 4 are the result of a chance coincidence. However, the combination of the four arguments strongly suggests that most of the bulge point sources are massive stars or small groups of a few massive stars or poor clusters whose energy distribution is strongly dominated by one or two massive stars. These are statistical arguments based on the whole sample of the bulge point sources. It is certainly possible that some of the point sources are in fact clusters instead of single or very small groups of stars. This is probably the case for the few most luminous hot objects with $L_* > 10^7\ L_\odot$ and certainly for object 21 with $L_* > 10^8\ L_\odot$.

6. THE STAR FORMATION RATE IN THE BULGE OF M51

If the point sources are single stars or small groups of stars, their age is very small and on the order of a few times 10^6 yr. Source 13 with $t \simeq 2 \times 10^7$ yr is the only exception. (Even if they are clusters, at least half of them are very young with ages less than 4×10^6 yr.) This clearly indicates the presence of ongoing formation of massive stars in the bulge. This is most likely related to the morphological structure of the bulge. The old background population of the bulge shows a smooth distribution of stars older than 5 Gyr (Paper I). However, the dust distribution shows evidence for spiral-like dust lanes. Figure 1 shows that these dust lanes in the bulge follow the same pattern and are the inner extensions of the dust lanes observed outside the bulge. One of the major dust lanes in the bulge can be traced down into the north side of the nucleus, and the other one can be seen to enter the nucleus on the south side. The bulge point sources also show evidence of occurring in strings with a morphology similar to that of the dust lanes. This shows that star formation is still going on in and near the spiral-like dust lanes in the bulge of M51.

The star formation rate in the bulge can be estimated only in a rough way. For this, we consider the group in the HR diagram of hot stars with $\log (L_*/L_\odot) > 5.5$ and the group of cooler stars with $\log (L_*/L_\odot) < 5.2$ separately. The group of point sources with $\log (L_*/L_\odot) > 5.5$ contains stars of initial mass in excess of 40 $M_\odot$. Their main-sequence lifetime is about 4×10^6 yr, depending only weakly on luminosity. With an age of 4×10^6 yr and a total mass of about 1400 $M_\odot$ (Fig. 6), the formation rate of these most massive stars in the bulge is $3 \times 10^{-4}\ M_\odot\ {\rm yr}^{-1}$.

We can also estimate the star formation rate from the 13 fainter point sources of $\log (L_*/L_\odot) < 5.2$, corresponding to stars in the initial mass range of 12–20 $M_\odot$. In this mass range we do not see the stars in the main-sequence phase because they will be too faint (see the lower limit in Fig. 6), but instead, we see them in the red supergiant phase. The red supergiant phase of stars in the range 12–20 $M_\odot$ lasts about 1.2×10^6 yr (1.6 Myr for 12 $M_\odot$ and 0.7 Myr for 20 $M_\odot$). The observed sources have a total initial mass of about 200 $M_\odot$. With this mass and an age range of 1.2×10^6 yr, we estimate the star formation rate of these lower mass stars to be about $2 \times 10^{-4}\ M_\odot\ {\rm yr}^{-1}$, i.e., of the same order of magnitude as found for the most massive stars. Taking both groups together, we find that in the mass range of about 12–120 $M_\odot$ the minimum star formation rate in the bulge is about $5 \times 10^{-4}\ M_\odot\ {\rm yr}^{-1}$. (In this estimate we did not include the mass of source 21, which is most likely an old cluster). This estimate provides obviously only a lower limit because we have assumed that only the most massive stars with $M > 12\ M_\odot$ are formed. In reality stars may be formed over a whole mass range down to some lower mass limit. This effect can be taken into account by assuming a continuous star formation with a given slope of the IMF: $-\Gamma \propto d(\log N)/(d \log m)$, where N is the number of stars per unit logarithmic mass interval. If we adopt $\Gamma = 1.35$ (Salpeter's value) with a lower limit of 1 $M_\odot$, we find a star formation rate of $2 \times 10^{-3}\ M_\odot\ {\rm yr}^{-1}$. If we adopt a flatter IMF of $\Gamma = 0.65$, we find a rate of $7 \times 10^{-4}\ M_\odot\ {\rm yr}^{-1}$.

We can derive a maximum star formation rate by assuming that all the bulge point sources are clusters and using the cluster masses and ages listed in Table 3. Taking the masses of the clusters formed in the last 10 Myr, we find a total mass of $1.6 \times 10^4\ M_\odot$ and a formation rate of $1.6 \times 10^{-3}\ M_\odot\ {\rm yr}^{-1}$. This is very similar to the rate derived under the assumption that all the point sources are young stars. This similarity is due to the very small masses of the

clusters, compared to the high mass of the stars, plus the correction for the presence of lower mass stars.

In Paper I we found that the bulge has a total dust mass of $2.3 \times 10^3\ M_\odot$. The gas content of the bulge in the form of neutral H has been derived from the 21 cm observations by Tilanus & Allen (1991). They find that the column density of neutral H in the bulge is much smaller than outside the bulge. In the inner 1′, i.e., within 240 pc from the nucleus, they measured a column density of 2×10^{20} H atoms cm^{-2}, with a maximum of 4×10^{20} (R. Allen 2001, private communication). This implies a total H I mass of $4 \times 10^5\ M_\odot$ and a gas-to-dust ratio of about 170, which is very close to the mean value of 140 ± 50 in the inner parts of our Galaxy (Cox 2000, p. 160). The estimate of the gas content excludes the contribution of the regions of high CO density within $4'' = 160$ pc from the nucleus found by Scoville et al. (1998), which have a total mass of about $10^7\ M_\odot$.

Adopting a total (gas + dust) content of $4 \times 10^5\ M_\odot$ and a star formation rate of $(1\text{–}2) \times 10^{-3}\ M_\odot\ \mathrm{yr}^{-1}$, we find that the bulge could sustain this star formation rate during about only $(2\text{–}4) \times 10^8$ yr. Interestingly, this is also the age of the starburst in the nucleus of M51 and approximately the time of closest approach of the companion (Paper I). This strongly suggests that the massive star formation in the bulge that we see now is fed by material that was brought into the bulge by the interaction of the two galaxies.

7. DISCUSSION

The most surprising result of this study is the presence of bright point sources in the bulge of M51 that is otherwise dominated by an old background stellar population and spiral-like dust bands of moderate optical depth [$E(B-V) \simeq 0.2$]. The energy distribution of the point sources shows that they are most likely isolated (or very small groups of) massive stars or very small clusters that are completely dominated by one or a few massive stars. The distribution of the point sources in the bulge of M51 in "strings" (see Fig. 4) shows that they are not ejected from the starburst in the nucleus but must have been formed in situ. This shows that massive stars do not necessarily form in clusters but that they can be formed as isolated stars or in very small groups. We compare this with several other regions of massive star formation and with theoretical predictions.

7.1. *Comparison with other Regions of Massive Star Formation*

We make the following comparisons with other regions of massive star formation:

1. The Orion Nebula cluster contains about 1600 optical stars with a total mass in excess of $10^3\ M_\odot$. We have shown in § 5.3.3 that the energy distribution of the ONC is much redder than that of the UV-bright sources in the bulge of M51. Only if there was no extinction at all in the ONC would its energy distribution be similar to that of the point sources in M51 with temperatures of about 25,000 K. However, the hotter M51 sources have a steeper energy distribution (equivalent to a higher temperature) than the ONC without extinction. This shows that these M51 sources have fewer (or no) low-mass stars than the ONC.

2. Brandl et al. (1995) and Brandl, Chernoff, & Moffat (2002) have shown that mass segregation has occurred in the core of the young compact LMC cluster R136a during the first few Myr. The massive stars are more strongly concentrated toward the center than lower mass stars. Stars of $M > 25\ M_\odot$ are concentrated within a core radius of 0.1 pc, which is 5 times smaller than the core radius of the whole cluster. Could our blue point sources be the cores of clusters? If the cluster R136a was in M51, we would not observe the mass segregation, and the photometry of the point source would include (almost) all stars in that cluster. So the "hot" energy distribution of many of the sources is not due to mass segregation unless the clusters in the bulge of M51 disperse on a very short timescale of a few Myr.

3. The bulge point sources in M51 can also be compared with the clusters that formed because of the interaction of the Antennae galaxies (NGC 4038/4039). Whitmore & Schweizer (1995) and Whitmore et al. (1999) identified point sources with magnitudes in the range of $-14 < M_V < -6$. The brighter ones are young globular clusters, and the lower luminosity objects could be stars or small clusters. This indicates cluster formation over the full mass range from $\sim 10^2$ to $10^6\ M_\odot$. This is different from the situation in the bulge of M51, where mainly isolated stars are formed.

7.2. *Comparison with Star Formation in Bulges of Other Spiral Galaxies*

We make the following comparisons with star formation in bulges of other spiral galaxies:

1. The inner part of our Galaxy, within a few parsecs from the nucleus, has several very young clusters with ages less than 4 Myr that contain massive stars. The best studied of these are the so-called Arches and Quintuplet clusters at a distance of about 30 pc from the Galactic center. However, these clusters have masses of 1×10^5 and $1 \times 10^4\ M_\odot$, respectively (Figer et al. 1998, 1999a; Figer, McClean, & Morris 1999b), which is much more massive than most of the bulge point sources in M51. Rich (1999) has suggested that the star formation near the Galactic center may favor the formation of massive stars because tidal forces may disrupt the clusters quickly, perhaps before the low-mass stars are formed.

2. A detailed study of the stellar population in the inner Galactic bulge, in Baade's Window, at a projected distance of about 400 pc from the center, shows that there is no evidence for the presence of luminous young stars with an age shorter than a few Gyrs (Frogel, Tiede, & Kuchinski 1999; Frogel 1999). This is different from M51, where we do find the young bulge sources at Galactocentric distances of several hundred parsecs.

3. Ichikawa et al. (1998) have shown that the mass-to-light ratios of bulges of nine spiral galaxies vary between 0.12 and 3.0 in the J band. This corresponds to stellar populations of ages in excess of 1 Gyr.

We conclude that there is little or no evidence for very young stars in bulges of galaxies other than M51, apart from the very center (within 20 pc) of our own Galaxy.

7.3. *Predicted Massive Star Formation in the Bulge of M51*

What are the conditions for the formation of massive stars outside clusters? Norman & Spaans (1997) and Mihos, Spaans, & McCaugh (1999) have studied the conditions for the formation of massive stars. They have suggested that

isolated massive stars can be formed in clouds in which H_2, [O I] 63 μm, and [C II] 158 μm are the dominant coolants. This occurs, for instance, in the vicinity of a hot ionizing source in a region with an optical depth $A_V \leq 1$ so that CO is dissociated but H_2 is protected by self-shielding.

It is very well possible that these following conditions are met in the bulge of M51:

1. The nucleus of M51 contains a starburst cluster with an initial mass of about $2 \times 10^7\ M_\odot$ within the central 17 pc (Paper I). The UV radiation field of such a cluster, a few 10^8 yr after the starburst, can be calculated with cluster evolution models (Leitherer & Heckman 1995). This yields a UV radiation field strength at a distance of about 200 pc of 10^2–10^3 in units of the mean radiation field in the Galaxy. Models calculated by one of us (M. S.) of the thermal and chemical structure of interstellar clouds that have 1 or 2 mag of visual extinction under these conditions show that CO is largely destroyed and that the [O I] fine structure line at 63 μm is the dominant coolant (M. Spaans 2002, in preparation).

2. The destruction of CO in clouds of small extinction and the increased photoelectric heating will result in relatively high cloud temperatures of 300–2000 K. This will lead to a high Jeans mass for gravitational contraction, and the McKee criterion of $A_V \sim 6$ (McKee 1989) to sustain star formation is not likely to be satisfied for the bulk of the gas. Since the low extinction causes any stellar source to induce disfavorable conditions for further star formation in its vicinity, isolated patches of forming stars are the natural state.

This suggests that the formation of isolated massive stars in the bulge of M51 could be due to the luminous central source, the low dust content, and the resulting small extinction. (The star formation under the conditions of the bulge of M51 will be described in more detail in M. Spaans et al. 2002, in preparation.)

8. CONCLUSIONS

We have studied bright point sources in the bulge of M51 with the *HST*-WFPC2 camera in six filters in the wavelength region of 2500–8200 Å. The results can be summarized as follows:

1. We found 30 point sources in the bulge of M51 with $21.38 < V < 26.20$. These point sources appear to occur in strings that follow the general pattern of the elliptical- or spiral-like dust lanes in the bulge of M51, but they do not necessarily coincide with the dust lanes.

2. The extinction of the point sources, derived by fitting their energy distribution with those of single-star models or cluster models, is in the range of $0 < E(B-V) < 1.3$. Half of the objects have $E(B-V) < 0.25$. The absolute visual magnitudes range from about $M_V \simeq -6$ to -9.

3. The energy distributions and the distribution of the point sources in the HR diagram suggest that most of them, except one or two, are stars rather than clusters because of the following:

a) The observed energy distributions better fit those of stellar models than those of cluster models.

b) Many of the sources have an energy distribution and a luminosity that is characteristic for a single hot massive star of $25{,}000\ \mathrm{K} \leq T_{\mathrm{eff}} \leq 50{,}000\ \mathrm{K}$.

c) The distribution of the objects in the HR diagram follows the Humphreys-Davidson luminosity upper limit for stars. There is no reason why clusters would follow this limit.

d) There is a gap in the distribution of the sources in the HR diagram at intermediate temperatures between $T_{\mathrm{eff}} \simeq$ 20,000 and 10,00 K. This is easily explained if the point sources are stars because that temperature range is crossed rapidly by the evolution tracks of stars. There is no obvious reason why clusters would avoid this temperature or color range.

4. The distribution of stars in the HR diagram shows two groups: (*a*) the most massive group of initial mass $M_i > 40\ M_\odot$ is mainly blue and hot because most of these stars will not evolve into red supergiants during their evolution and (*b*) the group with $12 M_\odot < M_i < 25\ M_\odot$ is mainly red and cool because stars in this mass range are below the detection limit during their main-sequence phase.

5. The current star formation rate in the bulge of M51 in the mass range of $12\ M_\odot < M < 200\ M_\odot$ is $\sim 5 \times 10^{-4}\ M_\odot\ \mathrm{yr}^{-1}$. Correcting for the possible presence of lower mass stars, down to $1\ M_\odot$, increases the star formation rate by a factor 3.4 if we adopt an IMF of slope $\Gamma = -1.35$ (Salpeter's value) and by a factor 1.5 if we adopt $\Gamma = -0.65$ (the value for the clusters near the Galactic center).

6. The total amount of neutral H in the bulge is about $4 \times 10^5\ M_\odot$, and the gas-to-dust mass ratio is about 150. The current star formation rate of about $2 \times 10^{-3}\ M_\odot\ \mathrm{yr}^{-1}$ can be sustained for about (2–4) $\times 10^8$ yr before all the gas is consumed. This suggests that this form of massive star formation in the bulge is fed/triggered by the interaction with the companion galaxy, whose closest approach was estimated to be about 4×10^8 yr ago.

7. These results show that under the conditions that exist in the bulge of M51, separate massive stars can form outside clusters or in very small groups. This agrees with the predictions of Norman & Spaan (1997), who argued that the formation of massive stars is favored in regions near a hot source (the core of M51) and small optical depth of $A_V \leq 1$ so that CO is dissociated but H_2 survives due to self-shielding. This may resemble the star formation in the early universe, when the CO content and the dust content were low due to the low metallicity.

H. J. G. L. M. L. is grateful to the Space telescope Science Institute for hospitality and financial support during various stays. We thank Ron Allen, Don Figer, Massimo Robberto, and Brad Whitmore for useful and stimulating discussions about 21 cm observation of M51, the clusters near the Galactic center, the Orion cluster, and star formation in the Antennae galaxies. Support for the SINS program GO 9114 was provided by NASA through a grant from the Space Telescope Science Institute, which is operated by the Association of Universities for Research in Astronomy, Inc., under NASA contract NAS 5-26555.

REFERENCES

Barnes, J. E. 1998, in Galaxies: Interactions and Induced Star Formation, ed. R. C. Kennicutt, Jr., F. Schweizer, F. E. Barnes, D. Friedli, L. Martinet & D. Pfenniger (Berlin: Springer), 275
Brandl, B., Chernoff, D. F., & Moffat, A. F. J. 2002, in IAU Symp. 207, Extragalactic Star Clusters, ed. E. K. Grebel, D. Geisler & D. Minniti (San Francisco: ASP), in press
Brandl, B., Drapatz, S., Eckart, A., Genzel, R., Hofmann, R., Loewe, M., & Sams, B. J. 1995, Messenger, 79, 23
Brocato, E., & Castellani, V. 1993, ApJ, 410, 99
Cassisi, S., Castellani, V., & Straniero, O. 1994, A&A, 282, 753
Cox, A. N. 2000, Allen's Astrophysical Quantities (New York: Springer)
Feldmeier, J. J., Ciardullo, R., & Jacoby, G. H. 1997, ApJ, 479, 231
Figer, D. F., Kim, S. S., Morris, M., Serabyn, E., Rich, R. M., & McLean, I. S. 1999a, ApJ, 525, 750
Figer, D. F., McClean, I. S., & Morris, M. 1999b, ApJ, 514, 202
Figer, D. F., Najarro, F., Morris, M., McLean, I. S., Geballe, T. R., Ghez, A., & Langer, N. 1998, ApJ, 506, 384
Fitzpatrick, E. L., & Garmany, C. D. 1990, ApJ, 363, 119
Frogel, J. A. 1999, in The Formation of Galactic Bulges, ed. C. M. Carollo, H. C. Ferguson, & R. F. G. Wyse (Cambridge: Cambridge Univ. Press), 38
Frogel, J. A., Tiede, G. P., & Kuchinski, L. E. 1999, AJ, 117, 2296
Garmany, C. D., Conti, P. S., & Massey, P. 1980, ApJ, 242, 1063
Gonzalez, R. A., Allen, R. J., Dirsch, B., Ferguson, H. C., Calzetti, D., & Panagia, N. 1998, ApJ, 506, 152
Hernquist, L. 1990, in Dynamics and Interactions of Galaxies, ed. R. Wielen (Heidelberg: Springer), 108
Hill, J. K., et al. 1997, ApJ, 477, 673
Hillenbrand, L. A. 1997, AJ, 113, 1733
Holtzman, J. A., et al. 1995, PASP, 107, 156
Humphreys, R. M., & Davidson, K. 1979, ApJ, 232, 409
Ichikawa, T., Itoh, N., Yanagisawa, K., & Sofue, Y. 1998, in IAU Symp. 184, The Central Regions of the Galaxy and Galaxies, ed. Y. Sofue (Dordrecht: Kluwer), 53
Krist, J. E., & Burrows, C. J. 1994, Appl. Opt, 34, 4951
Kurucz, R. L. 1993, Kurucz CD-ROM 13, ATLAS9 Stellar Atmosphere Programs and the 2 km s^{-1} Grid (Cambridge: SAO)
Leitherer, C., & Heckman, T. M. 1995, ApJS, 96, 9
McKee, C. F. 1989, ApJ, 345, 782
Meynet, G., Maeder, A., Schaller, G., Schaerer, D., & Charbonnel, C. 1994, A&AS, 103, 97
Mihos, J. C., Spaans, M., & McCaugh, S. S. 1999, ApJ, 515, 89
Millard, J., et al. 1999, ApJ, 527, 746
Norman, C., & Spaans, M. 1997, ApJ, 480, 145
Rich, R. M. 1999, in The Formation of Galactic Bulges, ed. C. M. Carollo, H. C. Ferguson, & R. F. G. Wyse (Cambridge: Cambridge Univ. Press), 54
Romaniello, M. 1998, Ph.D. thesis, Scuola Normale Superiore di Pisa
Savage, B. D., & Mathis, J. S. 1979, ARA&A, 17, 73
Scoville, N. Z., Yun, M. S., Armus, L., & Ford, H. 1998, ApJ, 493, L63
Scuderi, S., Capetti, A., Panagia, N., Lamers, H. J. G. L. M., & Kirschner, R. P. 2002, ApJ, submitted (Paper I)
Tilanus, R. P. J., & Allen, R. J. 1991, A&A, 244, 8
Toomre, A., & Toomre, J. 1972, ApJ, 178, 623
Whitmore, B. C. 1995, in Calibrating *HST*: Post Servicing Mission, ed. A. Koratkar & C. Leitherer (Baltimore: STScI), 269
Whitmore, B. C., & Schweizer, F. 1995, AJ, 109, 960
Whitmore, B. C., Zhang, Q., Leitherer, C., Fall, M., Schweizer, F., & Miller, B. W. 1999, AJ, 118, 1551
Williams, R. E., et al. 1996, AJ, 112, 1335